Inorganic Chemistry Communications 170 (2024) 113287

Contents lists available at ScienceDirect

Inorganic Chemistry Communications

journal homepage: www.elsevier.com/locate/inoche

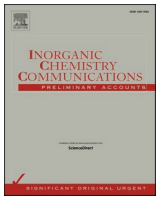

Short communication

Easy fabrication of PVA-CaO-CuO composite films for efficient photocatalyst: Towards distinct luminescence property, morphology and thermal stability

Mohammad Mizanur Rahman Khan [a,*], Nilave Chakraborty [b], Jae-Ho Jeong [a,*]

[a] Department of Mechanical, Smart and Industrial Engineering, Gachon University-1342, Seongnam-daero, Sujeong-gu, Seongnam-si, Gyeonggi-do 13120, Republic of Korea

[b] Department of Chemistry, University of Utah, 315 South 1400 East Salt Lake City, UT 84112-0850, USA

ARTICLE INFO

Keywords:
PVA-CuO-CaO composites
Optical transparency
Morphology
Thermal properties
Photocatalytic activity

ABSTRACT

PVA-CuO-CaO composites in the film form were synthesized by loading the different compositions of metal oxides (CuO and CaO) ranging from 5 to 25 wt% via solvent casting approach. The applications of the prepared composites as photocatalysts were assessed together with the findings of photoluminescence (PL) characteristics, optical clarity, morphological features, and thermal properties. Fourier-transformed infrared (FTIR), ultraviolet–visible (UV–vis), and photoluminescence (PL) spectra exposed the systematic and viableintegration of metal oxides (CuO-CaO) into the PVA matrix in PVA-CuO-CaO composites. The modifications of PL property of PVA-CuO-CaO composites were recognized rather than bare PVA. The prepared composite films exhibited excellent optical transparency irrespective of the addition of metal oxides. Both TGA and DSC data showed that the thermal properties of the composites could be significantly enhanced by incorporating CuO and CaO. DSC measurements demonstrated that the Tm of PVA-CuO-CaO composites is improved substantially (~7 to 38 °C) than PVA. The distinct morphological structures of the obtained composites were identified with variations in CuO and CaO addition remaining diameter in the 30–200 nm range. The photocatalytic assessments revealed the better photocatalytic performance of PVA-CuO-CaO composites for removing methylene blue (MB) than bare PVA. By eliminating organic pollutants, the current study may provide a new perspective on the preparation of water-processable PVA-CuO-CaO photocatalysts for wastewater management.

1. Introduction

Recently, wastewater containing organic pollutants has been a significant threat to human and aquatic life. The number of organic contaminants like dyes expelled daily from several industries such as textile, paper, pharmaceuticals, tannery, and bleaching industries, *etc*. is a warning issued for the current world, especially for developing countries. The dyes can remain unchanged in the environment for a long time. They mostly have a synthetic source and are based on complex aromatic structures thamake them stable and rigid to biodegrade [1]. Many trials have been conducted by researchers to develop an efficient material with appropriate wastewater treatment techniques to increase the efficacy of water purification., Techniques that have been used but not limited to removing dyes from wastewater include flocculation, adsorption, filtration, and photodegradation [2–4]. However, these wastewater treatment techniques have several drawbacks like low removal efficacy, and inadequate removal of dyes [5]. To mitigate these drawbacks, sunlight-induced photocatalytic process could be a great solution which can eliminate such toxic pollutants from the wastewater discharge from industries [6,7]. Thus, photodegradation is the emerging approach to eliminate organic dyes. Therefore, the field of photocatalysis has drawn strong interest due to its low cost, high efficiency, and absence of environmental secondary contamination [8]. Moreover, photocatalysis is a sophisticated oxidation process that relies on electron-hole pairs produced by photo absorption in semiconductor materials. Therefore, it is imperative to design and create novel materials, such as polymer composites, to use as a photocatalyst in the removal of organic dyes.

Polymers comprising metal oxides implanted in a host matrix can potentially develop remarkable features, including morphology and

* Corresponding authors.
E-mail addresses: mmrkhan@gachon.ac.kr (M.M. Rahman Khan), jaeho.jeong@gachon.ac.kr (J.-H. Jeong).

https://doi.org/10.1016/j.inoche.2024.113287
Received 9 August 2024; Received in revised form 18 September 2024; Accepted 4 October 2024
Available online 8 October 2024

thermal properties for certain applications like photocatalysts, sensors, *etc*., [9,10]. Among the polymers, PVA (−[-CH_2-CHOH-]n-) is used considerably for the synthesis of nanocomposites owing to its simple processability, exceptionally hydrophilic characteristics, proper film-forming abilities, and optical clearness [11]. Additionally, PVA can be employed as a host polymeric material to fabricate nanocomposites exploiting different kinds of semiconducting materials and metal oxides [11–13]. Such synthesis of PVA-based metal oxide composites can be accomplished through the solvent casting method with promising functionalities and for useful applications like wastewater treatment [11,14]. Different metal oxides such as TiO_2, ZnO, Fe_2O_3, Al_2O_3, and CuO have been successfully employed in PVA to produce composites for wastewater treatment until now [9,15–18].

The use of metal oxides as photocatalysts has achieved a noteworthy impact on the degradation of organic dyes [7,19]. So, researchers are attempting to introduce metal oxides with the polymers to create a novel photocatalyst to remove contaminated dyes from the wastewater [20,21]. Among the metal oxides, CuO is a very promising material as a photocatalyst to degrade organic dyes from contaminated water [23]. Further, CuO is a transition metal oxide that has already been used in different applications like chemical and gas sensors, high-temperature superconductors, and photocatalysis [22–24]. The bandgap of CuO is 1.5 eV and it is a p-type semiconductor [25]. These characteristics of CuO may be beneficial in increasing the photocatalytic performances in the form of a composite with the polymers. Similarly, as a metal oxide, CaO is inexpensive, highly basic that is also non-corrosive, benign to the economy, and simple to work with. Recently, CaO nanoparticles have been used as an active catalyst, such as to remove contaminated heavy metal ions in water and photocatalysts [26,27].Therefore, we hypothesize that combined use of these two metal oxides (CuO and CaO) may contrive a synergistic effect to and enhance the organic dye degradation capability of the photocatalysts compared to only one metal oxide.

Nowadays, to avoid the drawbacks of single metal oxide use in preparing nanocomposites, researchers have focused on the use of mixed metal oxides [9]. Such an attempt is beneficial because of the efficient charge separation that can be achieved by coupling two metal oxide particles with different energy levels and also to increase the efficiency of photocatalysts. For instance, the researcher synthesized PVA-ZnO-Al_2O_3 composites for efficient photocatalytic applications [9]. Considering the potential use of photocatalysts for the removal of organic dyes, adding CuO and CaO to PVA to develop PVA-CuO-CaO composites may be notable in this regard. Confirming the incorporation and interaction of CuO and CaO onto PVA may therefore be crucial, as this identification is required from an application perspective.

To the utmost of our acquaintance, no reports have been published on the fabrication of PVA-CuO-CaO composites whereby the optical, luminescence, morphology, and thermal characteristics of PVA are modified by simultaneously using CuO and CaO. Furthermore, no report can be found in the literature on the degradation of MB from wastewater utilizing PVA-CuO-CaO composite films as a photocatalyst. Moreover, it would be worthwhile to develop PVA-CuO-CaO composite films given the lack of literature on PVA-based PVA-CuO–CaO composites and their photocatalytic applications. In this instance, we describe a straightforward solvent casting technique for synthesizing PVA-CuO-CaO composite in the film form and their photocatalytic removal of MB in the presence of direct sunshine. The enhanced photoluminescence, thermal possessions, and unique morphological features of the fabricated composite films have also been testified in the extant work.

2. Experimental section

2.1. Materials

The chemicals were analytical category and were used as received. Polyvinylalcohol (PVA) (Mw = 72,000), Calcium oxide (CaO, 99.995 %), copper oxide (CuO, 99.995 %), and acetone ((CH_3)$_2$CO, ≥ 99.5 %) were attained from Sigma − Aldrich and were used without advance refinement.

2.2. Synthesis of PVA-CuO-CaO composite films

The PVA-CuO-CaO composite films were prepared following the modified procedure reported by the researchers [9]. Five distinctive synthesis batches were prepared by mixing a constant amount of 0.5 g PVA and five different ratios of CuO and CaO (5 to 25 wt%). These metal oxides were taken according to their weight percent relative to PVA weight and divided equally among them. More clearly, the compositions of CuO and CaO were taken keeping their amount 1:1 ratio for each weight percent (5-25 wt%) used in the synthesis process. Each sample was identified according to their weight percent as α, β, γ, δ, θ as presented in Table 1.

The polymer solution was made using a conventional method, which involved dissolving 0.5 g of PVA in 15 mL distilled water at 60 °C while vigorously stirring. To cast the solvent, the prepared solution was put into a vacuum rotary evaporator. In another flask, the required volume (weight percent) of metal oxides (CuO–CaO) for each synthesis batch was dissolved in water and subjected to two hours of sonication. After that, the metal oxides and PVA solution were combined in a rotary evaporator that was kept between 80 and 90 °C. Finally, the blend was placed into a glass petri dish and dried for a whole day at 30 °C. After solvent exclusion, air bubble-free, uniformly dispersed PVA films containing evenly distributed metal oxide particles were produced.

2.3. Characterization

FTIR spectra were attained by a Shimadzu FTIR spectrophotometer Prestige-21, functioning in the frequency range of 4000–400 cm^{-1}. The UV–visible data were taken using a Shimadzu UV-1800 with a 200–800 cm^{-1} range. FESEM/EDX experiments were accomplished on a JEOL JSM 7600F set with EDX. The platinum coating was used to make the sample for the FESEM experiment. Thermal analyses of PVA and PVA-CuO-CaO composites were performed by TGA exploitation a Shimadzu TGA-50 analyzer. Samples were heated in a platinum crucible between 25 to 850 °C for the measurements, with a heating rate of 10 °C/minute and a flow rate of 20 mL/minute of N_2. Using differential scanning calorimetry (DSC) in a Shimadzu TA-60A equipment, the glass transition temperatures (Tg), melting temperatures (Tm), and related enthalpies (ΔHm) during phase change were evaluated at 25 to 250 °C in a N_2 atmosphere. Both heating and cooling rates were possessed constant at 10 °C/min.

2.4. Photocatalytic investigations

The PVA-CuO-CaO nanocomposite films photocatalytic tests were carried out by treating MB in the presence of sunlight and following the approach according to the technique described in reference [9]. The use of direct sunlight irradiation for the photocatalytic experiments does not require any cost for the light source. The simple experimental set-up is already explained in reference [20]. In order o support similar irradiation power of sunlight, the investigations were conducted for each

Table 1
Synthesis identifier and composition of the CuO and CaO expended in synthesis process are listed:

Synthesis identifier	CuO and CaO addition (wt%)	Type of Product
PVA	–	PVA film
α	5 %	Composite film
β	10 %	Composite film
γ	15 %	Composite film
δ	20 %	Composite film
ε	25 %	Composite film

sample at an identical time and in the same environment. 20 mg of photocatalytic sample was suspended in MB solution for the tests ($C_0 = 2$ mg/L). The mixture was then constantly agitated for 30 min in a dark environment to reach the absorption–desorption balance between the photocatalyst sample and MB, prior to using the sunlight treatment. Following specified periods of exposure to sunlight illumination, the mixture aliquots were eradicated for centrifugation at 3000 rpm for 20 min. Following centrifugation, the obtained supernatant was exposed to UV–vis measurements to perceive the removal performance of MB. The distinct absorption signal of MB at 664 nm was utilized to determine the percentage of dye exclusion. Finally, degradation efficacy was recognized by exploiting the technique previously described in reference [9].

3. Results and discussion

3.1. FTIR spectra and analysis

FTIR analysis was carried out to comprehend the potential interaction between the PVA matrix and metal oxide (CuO-CaO) particles. Fig. 1 displays the FTIR peaks of PVA and PVA-CuO-CaO and the corresponding characteristic peaks are listed in Table 2. The O–H stretching vibration of PVA is attributed to a strong and broad absorption band at 3000–3600 cm^{-1}, peaking at 3343 cm^{-1}. A similar broader peak due to O–H stretching vibration was reported in reference [28]. At 2911 cm^{-1}, the band corresponding to C–H asymmetric stretching vibration was observed. Peaks identified at 1660 and 1712 cm^{-1} correspond to C = C stretching and C = O stretching vibration (vinyl acetate group of PVA), respectively. The signal at 1266 cm^{-1} is due to C–H wagging, while the strong peak at 1094 cm^{-1} is related to the stretching vibration of C–O in the C–O–H groups [29]. The CH_2 groups exhibited bending and wagging vibrations at 1435 and 1331 cm^{-1}, respectively. For all PVA-CuO-CaO composites, the occurrence of the symmetrical stretching vibration of the –OH group moved to an upper wave number (3374–3431 cm^{-1}) than PVA film, suggesting somewhat reduced hydrogen bonding with the PVA structure [6,8]. This type of interaction is mostly vital for the uniform dispersion of the CuO-CaO particles in the whole polymer matrix without letting agglomeration. In addition, the identification of characteristic peaksfor Cu–O and Ca-O at 632–418 cm^{-1} in PVA-CuO-CaO composite samples confirming the incorporation of CuO and CaO in the PVA matrix [30,31].

Table 2
Typical FTIR peaks PVA and PVA-CuO-CaO composites.

Peak designation	Peak values of the corresponding samples (cm^{-1})					
	PVA	α	β	γ	δ	ε
O–H stretching	3343	3431	3397	3383	3379	3374
C–H stretching	2911	2929	2926	2933	2942	2942
C═C stretching	1660	1645	1560	1564	1563	1546
C═O stretching	1712	1739	1720	1735	1715	1611
C–O stretching	1094	1091	1096	1092	1094	1094
C–H wagging	1266	1263	1265	1264	1267	1264
CH_2 bending	1435	1438	1436	1437	1448	1450
CH_2 wagging	1331	1262	1263	1261	1270	1233

3.2. UV–vis spectra and analysis

The room temperature UV–visible spectra of CuO, CaO, and PVA-CuO-CaO nanocomposite films are shown in Fig. 2. These UV–visible data were used to comprehend the integration of metal oxides with PVA structure in PVA-CuO-CaO composites. The corresponding band gap of these materials was determined using a UV–visible study. In this case, water was used as a solvent to record the UV–vis measurements.

The spectra show a broad absorption band around 275 nm for CuO and CaO (Fig. 2a), and its higher magnification graph is shown in the inset of Fig. 2b. In the case of PVA-CuO-CaO composites films, the absorption bands were identified at 353–340 nm (Fig. 2c) whereas, for PVA there is no peak found at the range 300–800 nm. PVA exhibits its typical band at 189 nm, as shown in our previous report [6]. This implies a bathochromic shift or red shift of UV–visible peaks from pure PVA and infers substantial incorporation of metal oxides (CuO-CaO) into PVA. Similar absorption bands due to the integration of PVA with metal oxides and/or nanoparticles were also previously reported in reference

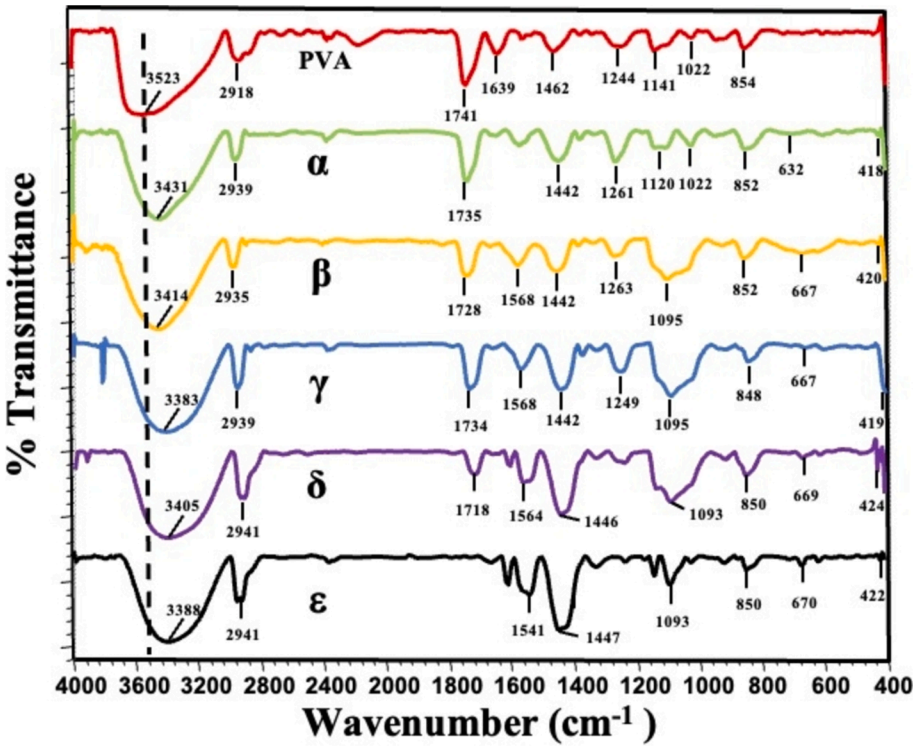

Fig. 1. FTIR spectra of PVA and PVA-CuO-CaO composites attained from distinctive synthesis batches α to ε.

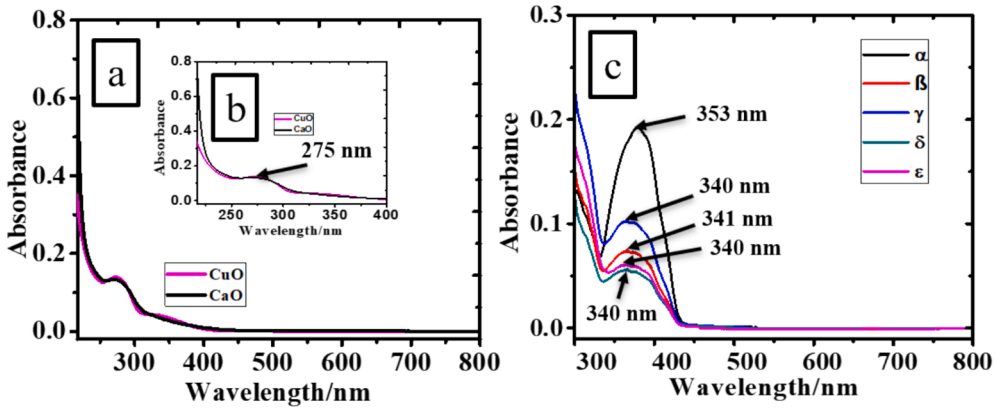

Fig. 2. UV–vis spectra of a) CuO and CaO, b) Magnified UV–vis spectrum of corresponding CuO and CaO samples (inset) to identify both the peaks more clearly, and c) PVA-CuO-CaO composite films.

[9,11,32].

The band gap of metal oxide and composites was estimated using the equation reported in reference [6,8]. The determined band gap of the PVA-CuO-CaO composites is 3.50 eV–3.65 eV, while the value for CuO and CaO is 4.54 eV and 4.59 eV, respectively [33,34]. The obtained band gap for CuO is greater than the value reported in the literature. However, such band gap variation for CuO with possible explanation is reported in reference [35]. Such variations in the band gap of metal oxides and composites denote their strong interaction in the matrix. Further, it is possible to anticipate from the band gap of composites that the incorporation of CuO and CaO with PVA significant impacted the light absorption [11]. This observation supports the idea that the presence of CuO and CaO may enhance the photodegradation ability of PVA-CuO-CaO composite films than PVA alone.

3.3. Effect of CuO and CaO on photoluminescence properties

PL measurements can provide additional evidence for the interaction between PVA and metal oxides.

Room temperature photoluminescence spectra of PVA and PVA-CuO-CaO composites at 350 nm excitation wavelength are shown in Fig. 3. PVA displayed a strong photoluminescence emission in visible range 325–400 nm, with a peak identified at 363 nm (Fig. 3a). The $\pi^* \rightarrow$ n electronic transition of –OH groups that results from the isotactic, syndiotactic, and atactic forms PVA molecules is caused by this emission [32]. As observed in Fig. 3c, the emission spectrum of CuO-CaO occurs at centered around 369 nm and 466 nm. Here, the peak observed at 369 nm corresponds to the near-band edge transition of metal oxides (CuO-CaO) [36]. The peak identified at 466 nm, may associated with the deep-level emission of metal oxides (CuO-CaO) that usually occurs in the case of semiconductive materials [37].

Two notable peaks identified at 367–370 nm and 466–468 nm for PVA-CuO-CaO composite samples correspond to shifts in syndiotactic and isotactic PVA, respectively (Fig. 3b). As a result, a peak emission corresponding to red shifting is noticed for all composites competed against PVA. These findings clearly show that CuO and CaO have been incorporated into PVA and such existence of CuO-CaO primarily reorganizes the delocalized n-electrons of –OH groups inside the PVA structure. These outcomes are in line with earlier studies [9,38]. Such types of materials (CuO, CaO) also have an impact on Stokes shift of PVA-CuO-CaO composites. The stokes shifts PVA-CuO-CaO composites were found at 17–29 nm. An analogous stoke shift of PVA-based materials was reported earlier, and it explained how the inorganic materials influence the stokes shift of PVA [39,40]. Thus, all of these results further indicate the interaction of CuO and CaO with PVA films.

3.4. Optical transparency

The optical clearness of prepared PVA-CuO-CaO films was realized by UV–visible spectroscopy (see Fig. 2). Composite films were explored in the wavelength range of 200–800 nm to assess optical transmission,. There is no absorption band in the visible region for all the composite films, demonstrating the very worthy optical transparency in the visible light limit [41]. The observed high optical transparency of PVA-CuO-CaO films makes them potential candidates for electrical devices as polarizer films.

To observe the optical transparency more clearly, the optical images of PVA and all composites were acquired, as shown in Fig. 4(a-f). The measured thickness of the films is about 145 μm and was placed on color fonts in print on paper. From the images, it is noticeable that the optical transparency of composite films is outstanding regardless of the extent of CuO-CaO addition in the synthesis process. However, with the increase in the addition of CuO-CaO into the PVA, slight decrease of the optical transparency further implies the formation of PVA-CaO-CuO

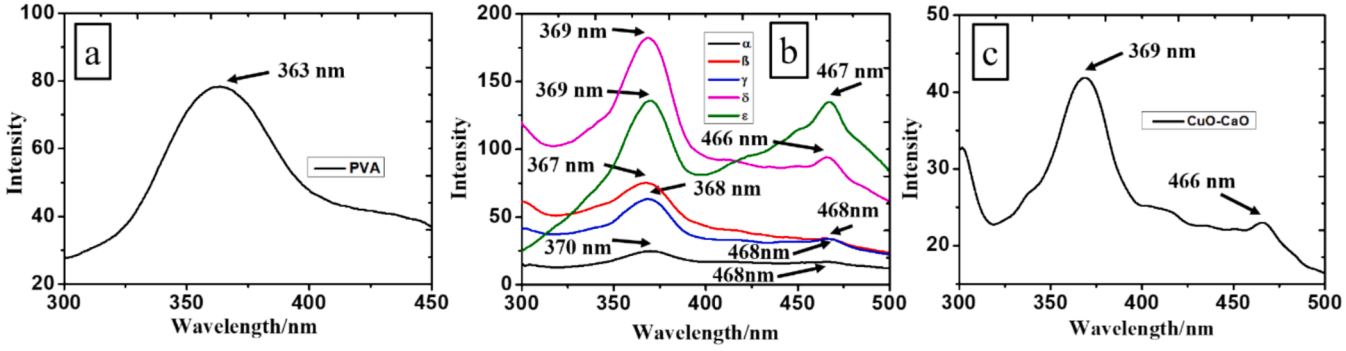

Fig. 3. PL data of (a) PVA, (b) PVA-CuO-CaO composites, and (c) CuO-CaO.

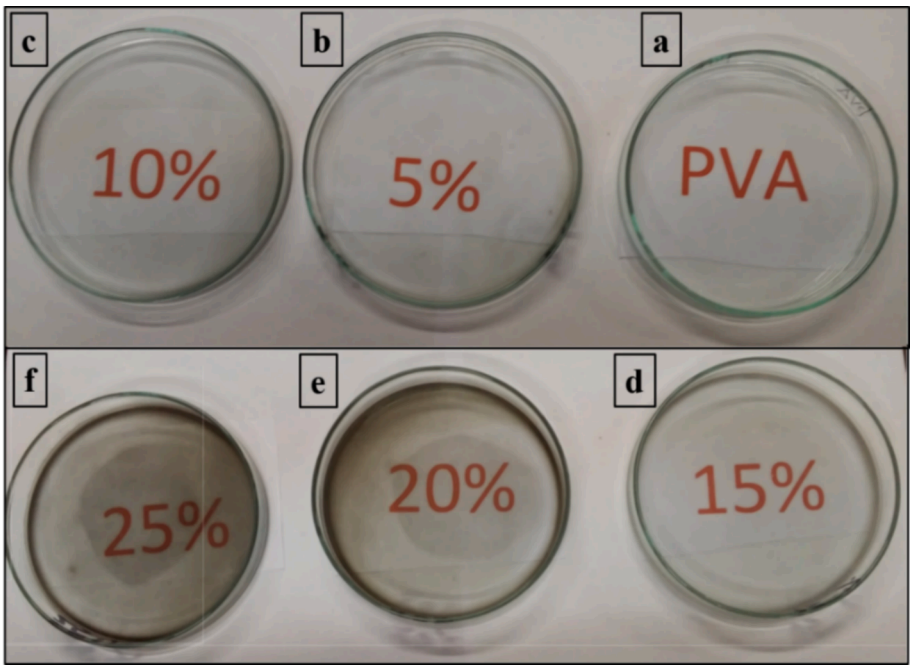

Fig. 4. Optical images of the a) PVA and b) PVA-CuO-CaO composite films. Panels (b-f) represent the composites synthesized at distinctive addition of CuO and CaO (5–25 wt%).

composite films.

3.5. Morphology of PVA-CuO-CaO composites

The morphological structures of the prepared composites were considered from their FESEM micrographs. For example, the representative FESEM images of PVA-CuO-CaO composites acquired from 5 wt%, 15 wt%, and 25 wt% are exhibited in Fig. 5(a-c). The images showed that composite films are comprised of nanostructures in the 30–200 nm range. For further understanding, the better enlargement images of respective composites are displayed in Fig. 5(d-f). In the case of lesser addition of CuO-CaO (5 and 10 wt%, synthesis batch α and β), the spherical-shaped composite structures are noticeable. The typical image is exhibited in Fig. 5a and its subsequent greater magnification data is shown in Fig. 5d. The higher rise of CuO-CaO amounts to 15 weights %, the composite shape is slightly elongated from their spherical shape (marked as a black circle) with sharp tails around the structure (Fig. 5b) which are more clearly visible in Fig. 5e; however, a few spherical shape

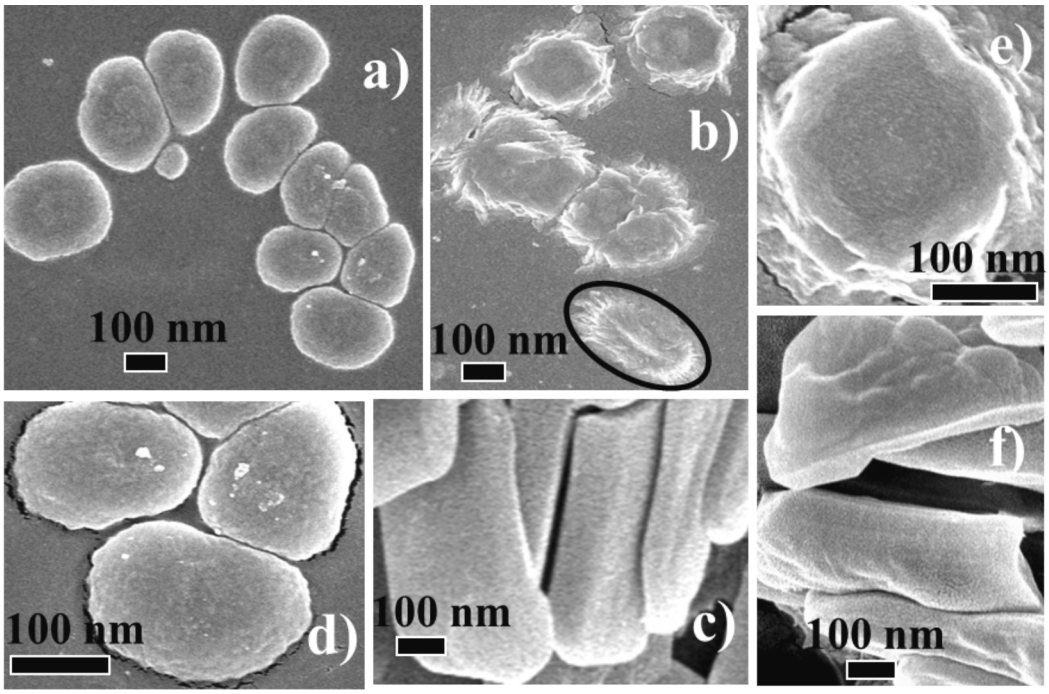

Fig. 5. FESEM image of (a) PVA-CuO-CaO composites (synthesis batch α, 5 wt% CaO-CuO addition), its (b) better magnification, (c) PVA-CuO-CaO composites (synthesis batch γ, 15 wt% CaO-CuO addition), its (d) enhance magnification, and (e) PVA-CuO-CaO composites (synthesis batch ε, 25 wt% CaO-CuO addition), its (f) higher magnification.

structures also remain at this stage. It seems the tendency to increment of length of the composite structure with the increase of metal oxide addition. These outcomes are steady with previous descriptions for polymer-based metal oxide composites [18,31]. Such tendency is also visible for the 20 wt% addition as presented in Fig. S1. For the highest 25 wt% addition of CuO-CaO (synthesis batch ε), the composite shape changes to a sheet-like structure with the increase of both length and diameter (Fig. 5c). The higher magnification image of such structure is located in Fig. 5f. Thus, for the higher addition of CuO-CaO, the composite morphology is changed from spherical shape to sheet-like structure. Such morphological changes with the inclusion of semiconducting materials with PVA are reported in reference [11]. Nonetheless, with the variation of the appropriate amount of CuO-CaO addition, the size and shape of the PVA-CuO-CaO composites can be controlled with the diameter range of 30–200 nm.

To intensify the analysis of incorporation of CuO-CaO with PVA together with the morphological reflections, EDX measurements were accomplished for PVA-CuO-CaO composites. For example, Fig. 6 exhibits the EDX spectrum of PVA-CaO-CuO composites obtained from synthesis batch ε (25 wt% CaO-CuO addition). Peaks of Ca and Cu together with the element C and O in the spectrum endorse their existence in the composites and supplement reasonably with FTIR and UV–visible evidence. An additional peak appears around 2.2 keV due to the presence of Pt. A similar peak position for the Pt is reported by other researchers [42]. This peak may arise due to the platinum coating of the sample used for FESEM/EDX measurements. From the EDX spectra, it is possible to observe for the composite sample, α that atomic % of Cu and Ca are 2.64 and 0.19, respectively (inset of Fig. 6). EDX results of the rest of the composite films are given in Fig. S2.

3.6. Thermal properties

The influence of metal oxides (CuO-CaO) on the thermal characteristics of the PVA was assessed by TGA investigation. Fig. 7 displays the TG curves for PVA and PVA-CuO-CaO nanocomposite films recorded in a nitrogen atmosphere. As seen from Fig. 7, the thermal degradation of PVA and the lowest addition (5 wt%) CuO-CaO samples (synthesis batch α) occurs in three distinct steps and for the higher addition (10 to 25 wt %) samples (synthesis batch β to ε) there are four distinct degradation steps are noticeable. The % of weight loss identified for each degradation step together with the respective temperature range is listed in Table 3.

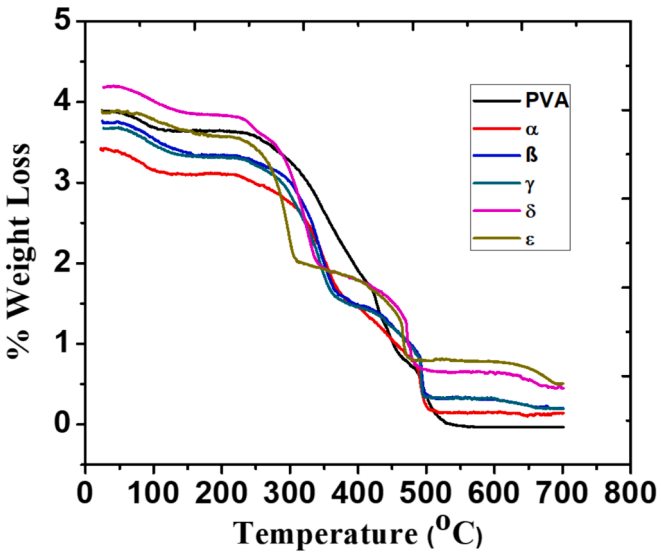

Fig. 7. TGA curves of PVA and PVA-CuO-CaO composites (α-ε).

The weight loss for the first degradation step is attributed to the removalof physically absorbed moisture and partial dehydration of PVA Chains [43]. A similar degradation step owing to the removal of physically absorbed moisture from the materials is reported in reference [44,45]. The corresponding % of weight loss is found at 5 % and 6 %–11 % for PVA and PVA-CuO-CaO nanocomposites films, respectively (Table 3). For PVA the second degradation steps are observed at 226–393 °C and the corresponding weight loss is 44 %, while for the composites such degradations are identified at 211–380 °C and the weight losses are 43–48 %. The second degradation step signifies the heating settlement of the polymer composition [46]. Third degradation step is seen for PVA and PVA-CuO-CaO composites are 395–518 °C and 331–514 °C, respectively, related to the disintegration temperature of PVA [47]. The mass loss at this stage is 48 % for PVA and 28–39 % for all composite samples. It was observed that the weight loss decreased for all composites demonstrating the improved thermal stability of PVA-CuO-CaO composites compared to pristine PVA. The cause of improved thermal stability of composites is due to the inclusion of CuO-CaO with PVA matrix. The addition of metal oxides into PVA may constrain the mobilities of polymer chains resulting in the lowering of mass loss for

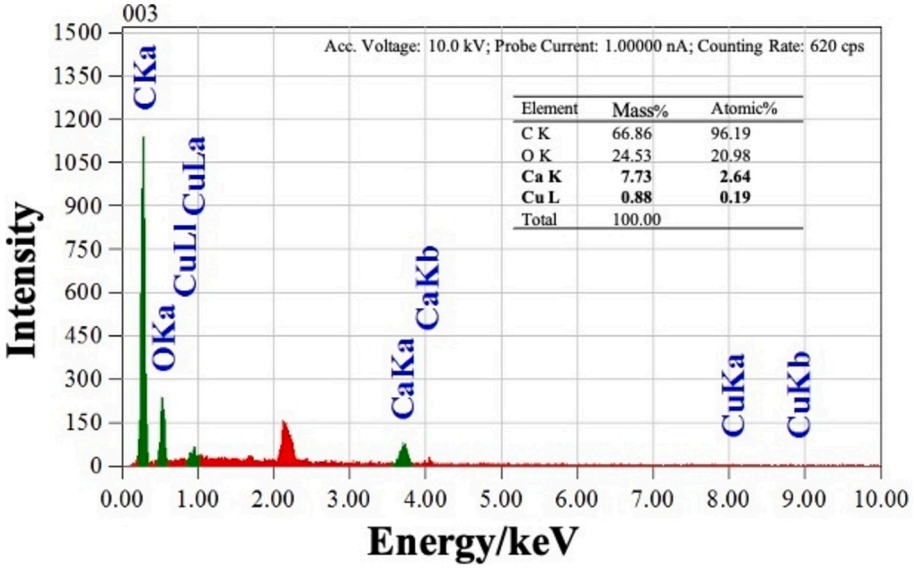

Fig. 6. EDX spectrum of PVA-CuO-CaO composites obtained from synthesis batch ε (5 wt% CaO-CuO addition).

Table 3
TGA data for PVA and PVA-CuO-CaO composites.

Sample	Temperature (T) and % of weight loss (WL) at four different steps								
	First step		Second step		Third step		Fourth step		Residual weight (%)
	T (°C)	WL (%)	Temp.	WL (%)	T (°C)	WL (%)	T (°C)	WL (%)	
PVA	46–108	5	226–393	44	395–518	48	–	–	3
α	49–105	7	223–380	44	386–514	39	–	–	10
β	49–151	11	213–356	44	357–487	33	479–789	7	5
γ	47–117	8	211–361	48	363–487	33	584–770	6	5
δ	47–124	7	212–330	43	331–484	31	483–798	8	11
ε	68–186	7	205–344	43	348–506	28	585–760	8	14

composites, which ultimately endures a relaxed disintegration progression [48]. Such effects correspond well with the enhancement of the thermal stability character of PVA-CuO-CaO composites due to the inclusion of oxide materials with the PVA [9]. A sudden weight loss was observed at the fourth step for the composite samples prepared with the higher addition (10 to 25 wt%) of metal oxides. The degradation temperature and weight losses are 479–798 °C and 6–8 %, respectively. Such disintegration step is instigated by the further breakdown of the polymer assembly consequently endures decomposition with the development of carbonaceous matter and persists continually, providing the plateau line in the TGA graph [49]. No discernible discrepancy of weight losses was found in the composite samples except for the sample synthesized from the least amount of PVA (5 wt%) where the fourth degradation phase did not occur like PVA.

The TGA results of the PVA-CuO-CaO composites revealed a residual mass that was estimated to be 5 to 14 %, whereas the identified mass for PVA films was very low at 3 %. The obtained residual mass is ascribed to the existence of non-disintegrated polymer chains, alkenes, and other organic molecules [46]. The presence of higher residual mass for the composite sample may be because the inorganic metal oxides (CuO-CaO) can function as a catalyst surface that inhibits the breakdown or basically the integration of metal oxides with PVA composed the composites disallowed to condensation-degradation process. Hence, according to the TGA data, the thermal stability of PVA-CuO-CaO composites has been significantly increased by the addition of CuO-CaO. Among the PVA-CuO-CaO samples, the greater residual value of 14 % identified for the highest addition of CuO-CaO synthesis batch, ε indicates its better thermal stability nature compared to other samples.

The DSC thermograms of PVA and PVA-CuO-CaO composites are presented in Fig. 8. Table 4 lists the obtained glass transition temperature (T_g), melting temperature (T_m), melting enthalpy (ΔH_m), and crystalline behavior of the corresponding samples. During the heating cycle, both PVA and PVA-CuO-CaO nanocomposite films display comparable thermal responses with three evident features as a function of temperature. The first peak is ascribed to the T_g recognized at 45.78°C and 34.96–40.24°C for PVA and PVA-CuO-CaO composites, respectively. Because of the presence of moisture, the T_g value for PVA is lower than that of its typical value [50].

Table 4
The melt onset temperature, T_g, T_m, ΔH_m, and crystallinity (X_c) of PVA and PVA–CuO-CaO composites are listed.

Sample	Melt OnsetTemperature (° C)	T_g (° C)	T_m (° C)	ΔH_m (J/g)	Crystallinity X_c (%)
PVA	169.90	45.78	191.40	32.21	23.24
α	181.25	38.68	198.43	35.88	25.89
β	189.72	34.96	208.38	36.26	26.16
γ	199.20	36.79	218.15	30.51	21.83
δ	210.43	40.24	221.60	16.96	12.23
ε	215.07	37.50	229.50	15.92	11.49

The incorporation of CuO-CaO nanoparticles decreased the T_g value of PVA in PVA-CuO-CaO samples. The cause of this decline may be due to the aggregation of CuO-CaO nanoparticles, which weakens the polymeric network strength and intermolecular connection between PVA chains [9,11,46]. The second peak was identified at 84.85°C and 78.3–110 °C for PVA and composite samples, respectively. This peak is designated to the thermal effect due to moisture evaporation from the materials and hydrogen-bonded water [9]. The third one pertains to the melting of the crystallites of the polymer network and is represented by the melting temperature (T_m) found at 191.40 °C for PVA, which increases from 198.43 °C to 229.50° C for PVA-CuO-CaO composite samples with the increase of composition of CuO-CaO from 5 to 25 wt% (Fig. 8b). This is due to the reduced mobility of the polymer chains after being attached to the metal oxides particle surface. The significant difference in melting temperature (T_m) between the pure PVA and the PVA-CuO-CaO indicates the significant interaction between metal oxides and –OH groups of PVA in composites [9,48].

From the DSC curve, calculating the degree of crystallinity is an essential technique for comprehending the changes in the structural features impacted by CuO-CaO. The following equation was utilized to evaluate the degree of relative crystallinity of the PVA and PVA-CuO-CaO composites [9]:

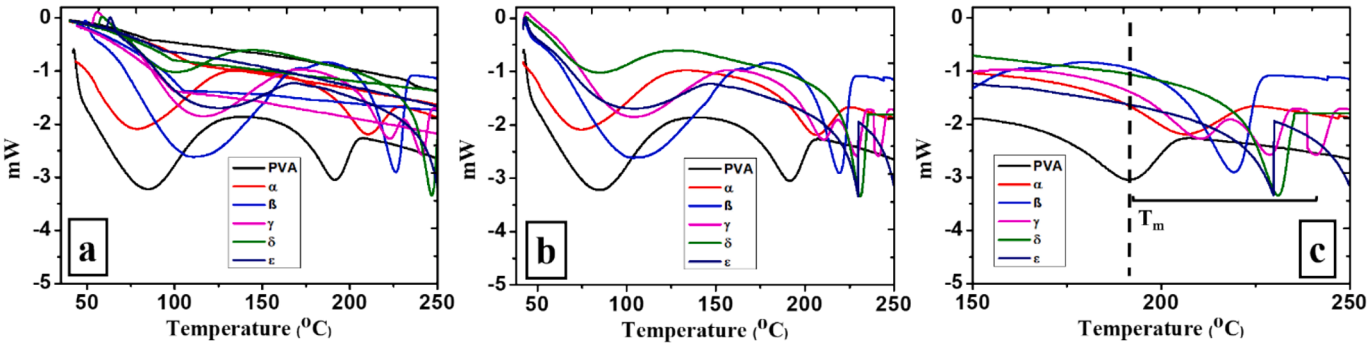

Fig. 8. DSC curves of (a) PVA and PVA-CuO-CaO composites (α-ε) for both the heating and cooling cycles. (b) Theromograms of corresponding samples only for heating cycles. (c) magnified thermograms displaying the melting temperature (T_m) of respective samples for better clarity.

$X_c = (\Delta H_m/\Delta H_{mo}) \times 100$

Where Xc denotes the degree of crystallinity, ΔHm is the enthalpy of melting achieved from the DSC curve, and ΔHm_o is the enthalpy of melting of 100 % crystalline PVA (ΔHm_o is 138.6 J/g) [51]. The assessed value of ΔH_{mo} for PVA was 32.21 J/g and the calculated degree of crystallinity was 23.24 %. The ΔH_m values are from 15.92 to 36.26 J/g for PVA-CuO-CaO composites, corresponding to the crystallinity 11.49–26.16 %. The determined degree of crystallinity of PVA and PVA-CuO-CaO composites is listed in Table 3. It is seen that the crystallinity slightly increases for the lower addition of metal oxides (5–10 wt%); however, the degree of crystallinity decreases for the higher loadings (15–25 wt%). The increasing trend of the degree of crystallinity leads to decreasing amorphization, while the decreasing trend is associated with an increase in amorphization. Such a change in crystallinity suggests the certainty of integration between PVA and CuO-CaO, which in turn leads to the reduction in contacts with polymer network [52].

3.7. Photocatalytic performances

The samples of CuO-CuO, PVA, and all PVA-CaO-CuO composites were tested by the photodisintegration of MB under direct sunlight treatment. Composite film's water resistivity was tested at various temperatures and found to be water resistant up to 67 °C, which is lower than the temperature commences from the sunlight illumination [11]. Fig. 9 and Fig. 10 depict the UV–vis absorption spectra illustrating the disintegration of MB using CuO-CaO, PVA, and PVA-CaO-CuO composites as a photocatalyst, respectively. From the absorption spectra of these materials, it can be seen that the absorption bands are diminishing as the time interval increases, exhibiting an efficient removal of MB for the corresponding samples (Fig. 9 and Fig. 10). The UV–vis spectra of MB encompassing 20 mg of CuO-CaO in direct sunlight illumination at various time intervals are shown in Fig. 9a. A similar type of time intervals for the removal of MB using PVA-based composite materials was reported in reference [11,53]. It was identified that absorption maxima dropped progressively as the irradiation period increased, and 100 % removal ensued after only 120 min of time extent. A similar outcome for the removal of organic dyes was identified by other researchers utilizing metal oxide-based materials [54–56]. For instance, a 97 % removal of RhB was observed using $Ce_{0.95}Fe_{0.05}O_2$/NiO/rGO (CFN-rGO) materials in 130 min of sunlight irradiation, 80.5 % removal of crystal violet and 42 % removal of phenol was observed using ZnO and $NiFe_2O_4$ in 140 min exposure time of sunlight [54,55]. When PVA film was used, only 65 % of the MB was removed after 480 min (Table 5), demonstrating its poor capacity for degradation (Fig. 9b). Similar behavior of PVA film for the removal of MB was reported in reference [11].

The PVA-CuO-CaO composite samples were applied as a photocatalyst, exploiting the identical experimental atmosphere to assess the photocatalytic potential of bare CaO-CuO and PVA. It is evident from Fig. 10 (a-e) that the absorption maxima drops gradually over specified time intervals for the PVA-CuO-CaO samples. Such a gradual decline shows the substantial blue shift which eventually approaches close to zero over the course of 480 min of solar radiation. Notably, no discernible disparity of absorption maxima was seen among the composites (Fig. 10 (a-e)). The apparent shift in absorption maxima of composites reveals the enduring adsorption of MB to samples and eventually approaches full degradation. Such PVA-CuO-CaO composite films are reusable up to 3 times for the removal of MB as shown in Figure S3. Relating to the mechanism and possible explanation of the removal of MB using PVA-based composite materials was previously reported in reference [11].

As shown in Table 5, the composite samples obtained from the synthesis batch (α-ε) showed 98.15–99.44 % dye removal after 480 min that are far better than the PVA film. Such outcomes are consistent with the previous reports for the removal of MB utilizing PVA-based composites [57,58] Thus, these findings indicate that the PVA-CuO-CaO composites can act as an excellent photocatalyst for the degradation of organic dyes compared to bare polymers. Therefore, a considerable synergistic enrichment outcome of the photocatalyst was identified for composites. This is owing to the notable interplay between the metal oxides (CuO-CaO) and PVA matrix. The similar impact of inorganic materials with the PVA for the removal of MB was testified by other researchers [9,11].

3.8. Kinetic studies

The reaction kinetics was studied for the degradation of methylene blue (MB) solution by observing the UV–vis absorbance data under sunlight irradiation. For this study, a pseudo-first-order kinetic model was examined. From Fig. 10 (a-e), it is obvious that the concentration of MB decreases linearly as a function of sunlight illumination time. The corresponding % of MB removal after a certain time interim is listed in Table 5. These data are useful for the kinetic model of MB degradation using the equation (1). This equation was used by other researchers to examine the pseudo-first-order kinetic model for MB degradation [59].

$$-\ln([C]/[C]_0) = k_{obs}\, t \quad (1)$$

Where $[C]_0$ represents the initial concentration of MB (mg/l), [C] is the concentration of MB at a certain reaction time, t (min), and k_{obs} is the rate constant of pseudo-first equation (m^{-1}). So. a plot of the $-\ln([C]/[C]_0)$ vs. time is presented in Fig. 11, from where the obtained results of rate constate, k_{obs} and the correlation coefficients, R^2 for pseudo-first equation can be appreciated. The value of k_{obs} is found as 0.0084 min^{-1}, 0.0094 min^{-1}, 0.0083 min^{-1}, 0.0098 min^{-1}, and 0.0107 min^{-1} for composite sample, α, β, γ, δ and ε, respectively. It was observed that

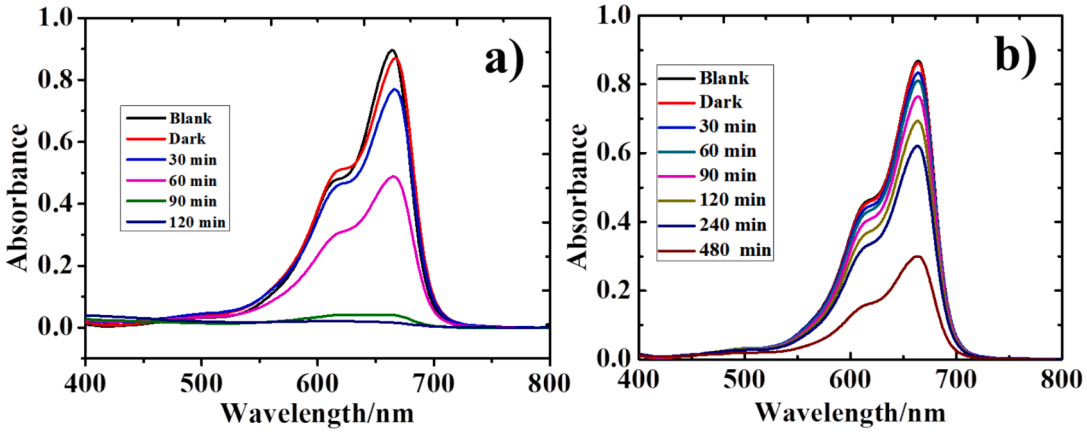

Fig. 9. Variations in the UV–vis spectra of MB solution by a) CuO-CaO and b) PVA films.

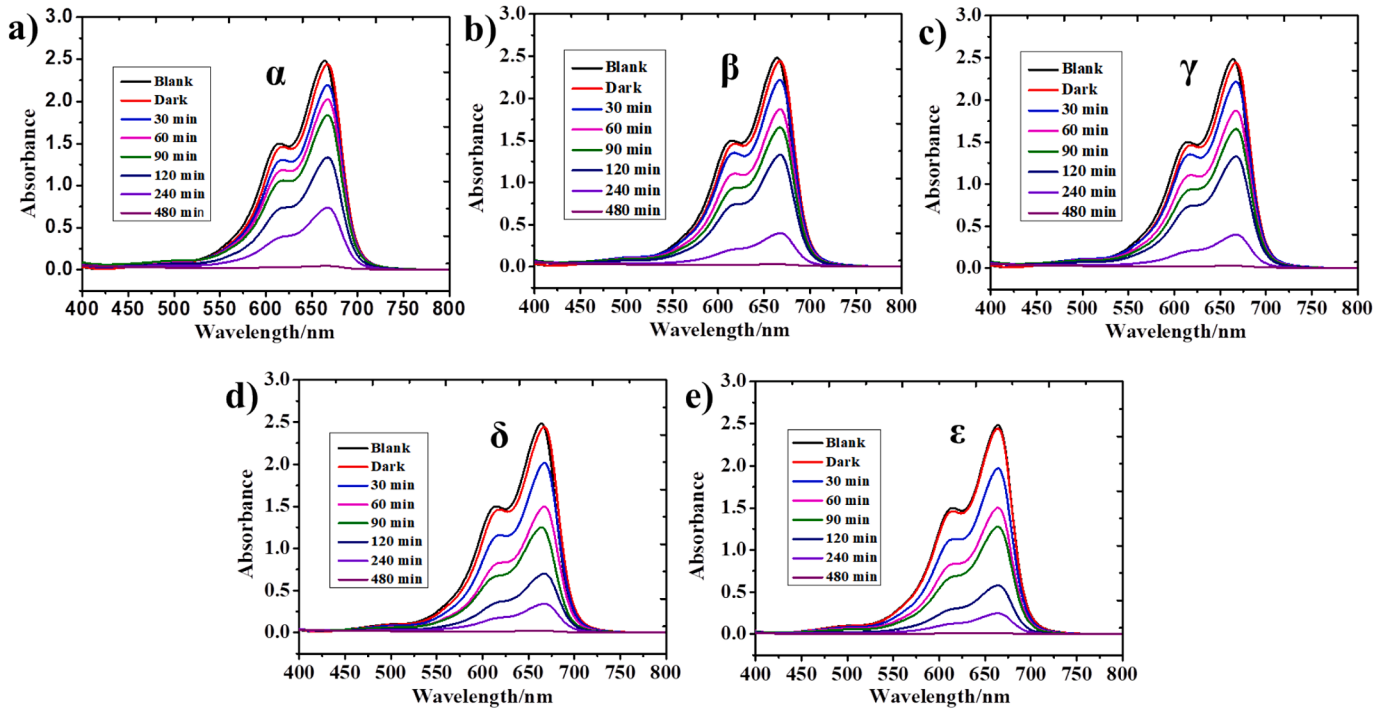

Fig. 10. (a-e) Variations in the UV–vis spectra of MB solution in the existence of PVA-CuO-CaO composite films (α-ε).

Table 5
The % of MB removal pertaining to irradiation time of sunlight treatment for all samples are listed:

Sample	% of removal in different time intervals (in minutes)					
	30	60	90	120	240	480
CaO-CuO	10.06	45.54	95.65	98.43	–	–
PVA	4.02	6.67	11.96	20.13	28.53	65.47
α	11.68	18.49	26.10	46.23	70.24	98.18
β	10.71	24.53	33.31	46.44	83.93	98.87
γ	10.87	24.57	33.35	46.48	84.09	98.91
δ	18.85	39.63	49.66	71.81	86.19	99.15
ε	20.74	39.63	48.65	76.60	89.97	99.44

the rate constant is higher for the composite sample ε prepared with the higher loading of CuO-CaO Fig. 11). Similar behavior of the rate constant for the degradation of MB was reported in reference [59].

4. Conclusions

PVA–CuO-CaO composite films were successfully fabricated by adding varying amounts of CuO and CaO with effective photocatalytic performance using the solvent casting method. The results of FTIR, UV–vis, and PL spectroscopy demonstrated the strong interaction of metal oxides (CuO and CaO) with PVA. The better photoluminescence property of PVA-CuO-CaO composites was seen than PVA alone. The optical transparency of the composite samples was superb. TGA data

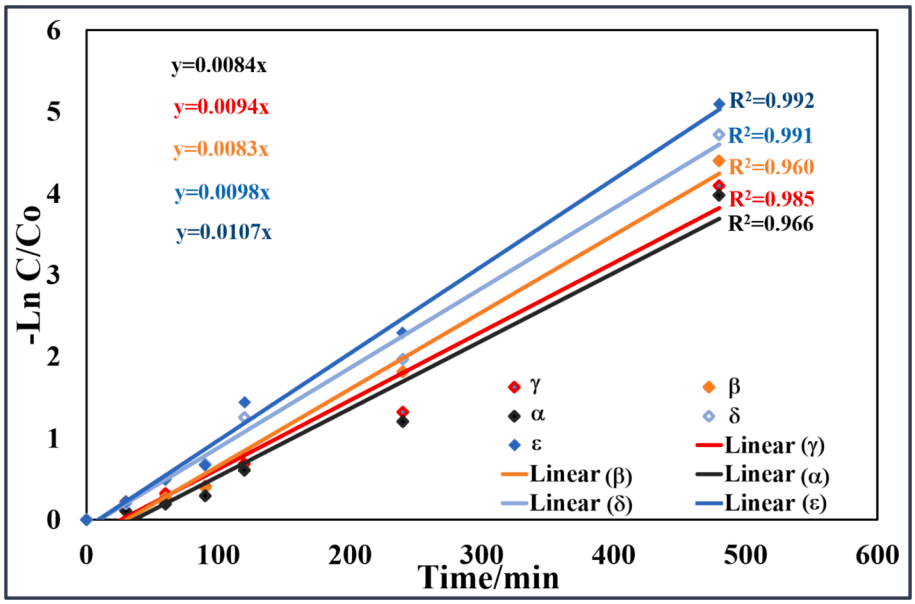

Fig. 11. Plot of pseudo first-order model for MB degradation using PVA-CaO-CuO composite films under solar irradiation (C_0 = 2 mg/L).

revealed 28–39 % weight loss for the PVA-CuO-CaO composites significantly lower than PVA (48 %). Such a substantial decline in weight loss displayed the enhanced thermal stability of the prepared composite films. The melting temperature (T_m) of composites could be greatly enhanced by ~ 7 to 38 °C compared to the polymer. The morphological distinction was observed for composite samples with diameters in the range of 30–200 nm. The photocatalytic enactment showed the superb photocatalytic activity of PVA-CuO-CaO composites for the degradation of MB compared to PVA owing to the inclusion of CuO and CaO into the PVA. All of these results provide straight evidence for the modification of photoluminescence, morphological features, and thermal properties of PVA-CuO-CaO composites. Additionally, photocatalytic capability exhibits a promising prospect in the fabrication of PVA-CuO-CaO photocatalysts for wastewater treatment.

CRediT authorship contribution statement

Mohammad Mizanur Rahman Khan: Writing – original draft, Validation, Supervision, Methodology, Investigation, Conceptualization. **Nilave Chakraborty:** Validation, Investigation, Data curation. **Jae-Ho Jeong:** Writing – review & editing, Validation, Investigation, Data curation.

Declaration of competing interest

The authors declare that they have no known competing financial interests or personal relationships that could have appeared to influence the work reported in this paper.

Data availability

Data will be made available on request.

Acknowledgements

The authors wish to express gratitude to the Department of Mechanical Engineering, Gachon University, for supporting the works. This work was supported by the Nuclear Safety Research Program through the Regulatory Research Management Agency for SMRS(RMAS) and the Nuclear Safety and Security Commission (NSSC) of the Republic of Korea (No. 1500-1501-409). This work was additionally supported by a National Research Foundation of Korea (NRF) grant funded by the Korea government (MSIT) (No. 2021M2E2A2081062).

Appendix A. Supplementary data

Supplementary data to this article can be found online at https://doi.org/10.1016/j.inoche.2024.113287.

References

[1] R. Al-Tohamy, S.S. Ali, F. Li, K.M. Okasha, Y.A.G. Mahmoud, T. Elsamahy, H. Jiao, F. Yu, J. Sun, A critical review on the treatment of dye-containing wastewater: Ecotoxicological and health concerns of textile dyes and possible remediation approaches for environmental safety, Ecotox. Environ. Safety. 231 (2022) 113160, https://doi.org/10.1016/j.ecoenv.2021.113160.

[2] T. Aarthi, G. Madras, Photocatalytic Degradation of Rhodamine Dyes with Nano-TiO_2, Ind. Eng. Chem. Res. 46 (2007) 7–14, https://doi.org/10.1021/ie060948n.

[3] N. Nikooe, E. Saljoughi, Preparation and characterization of novel PVDF nanofiltration membranes with hydrophilic property for filtration of dye aqueous solution, Appl. Surf. Sci. 413 (2017) 41–49, https://doi.org/10.1016/j.apsusc.2017.04.029.

[4] S. Mallakpour, F. Motirasoul, Capturing Cd^{2+} ions from wastewater using PVA/a-MnO_2–oleic acid nanocomposites, New J. Chem. 42 (2018) 4297–4307, https://doi.org/10.1039/C8NJ00304A.

[5] M. Siddiq, A.G. Taki, M. Aadil, S. Mubarik, E.W. Cochran, S. Zulfiqar, A.A. A. Mohammed, S. Ijaz, Microwave-assisted synthesis of tentacles like Ag-doped copper oxide nano- ceramics: Structural, optical, and anti-campylobacter studies, Ceramics Int. 49 (2023) 36590–36599, https://doi.org/10.1016/j.ceramint.2023.08.342.

[6] M. Aadil, W. Hassan, H.H. Somaily, S.R. Ejaz, R.R. Abass, H. Jasem, S.K. Hachim, A.H. Adhab, E.S. Abood, I.A. Alsafari, Synergistic effect of doping and nanotechnology to fabricate highly efficient photocatalyst for environmental remediation, J. Alloys Comp. 920 (2022) 165876, https://doi.org/10.1016/j.jallcom.2022.165876.

[7] T. Li, M. Aadil, S. Zulfiqa, A. Anwar, S.M. Yakout, N.M. Panduro-Tenazoa, S. Mubeen, Synthesis of doped and porous CuO with boosted light-harvesting features for the photocatalytic mineralization of azo dyes, Ceramics Int. 49 (2023) 27827–27836, https://doi.org/10.1016/j.ceramint.2023.05.272.

[8] M. Hussain, M. Ahmad, A. Nisar, H. Sun, S. Karim, M. Khan, S.D. Khan, M. Iqbal, S. Z. Hussain, Enhanced photocatalytic and electrochemical properties of Au nanoparticles supported TiO_2 microsphere, New J. Chem. 38 (2014) 1424–1432, https://doi.org/10.1039/C3NJ01525D.

[9] M.M. Rahman Khan, M. Akter, M.K. Amin, M. Younus, N. Chakraborty, Synthesis, luminescence and thermal properties of PVA–ZnO–Al_2O_3 composite films: Towards fabrication of sunlight-induced catalyst for organic dye removal, J. Polym. Environ. 26 (2018) 3371–3378, https://doi.org/10.1007/s10924-018-1220-9.

[10] X.J. Zhang, G.S. Wang, Y.Z. Wei, L. Guo, Polymer-composite with high dielectric constant and enhanced absorption properties based on graphene–CuS nanocomposites and polyvinylidene fluoride, J. Mater. Chem. A. 1 (2013) 12115–12122, https://doi.org/10.1039/C3TA12451G.

[11] M.M. Rahman Khan, S. Pal, M.M. Hoque, M.R. Alam, M. Younus, H. Kobayashi, Simple Fabrication of PVA–ZnS composite films with superior photocatalytic performance: Enhanced luminescence property, morphology, and thermal stability, ACS Omega. 4 (2019) 6144–6153, https://doi.org/10.1021/acsomega.8b02807.

[12] R.V. Kumar, Y. Koltypin, Y.S. Cohen, D. Aurbach, O. Palchik, I. Felner, A. Gedanken, Preparation of amorphous magnetite nanoparticles embedded in polyvinyl alcohol using ultrasound radiation, J. Mater. Chem. 10 (2000) 1125–1129, https://doi.org/10.1039/B000440P.

[13] X.F. Qian, J. Jin, J.C. Huang, Y.F. Yang, X.X. Guo, Z.K. Zhu, The preparation and characterization of PVA/Ag_2S nanocomposite, Mater. Chem. Phys. 68 (2001) 95–97, https://doi.org/10.1016/j.matchemphys.2005.05.050.

[14] A. Lagashetty, S. Basavaraj, M. Bedre, A. Venkatarman, Metal oxide dispersed polyvinyl alcohol nanocomposites, J. Metal Mater. Sci. 51 (2009) 297–306.

[15] R. Asahi, T. Morikawa, T. Ohwaki, K. Aoki, Y. Taga, Visible-light photocatalysis in nitrogen-doped titanium oxides, Science. 293 (200) 1269-271. DOI: 10.1126/science.1061051.

[16] M. Anbuvannan, M. Ramesh, G. Viruthagiri, N. Shanmugam, N. Kannadasan, Synthesis, characterization and photocatalytic activity of ZnO nanoparticles prepared by biological method, Spectrochim. Acta A. 143 (2015) 304–308, https://doi.org/10.1016/j.saa.2015.01.124.

[17] G. Jung, H. Kim, Synthesis and photocatalytic performance of PVA/TiO_2/graphene- MWCNT nanocomposites for dye removal, J. Appl. Polym. Sci. 131 (2015) 1–7, https://doi.org/10.1002/app.40715.

[18] M.M. Rahman Khan, Y.K. Wee, W. a. k., Mahmood Effects of CuO on the morphology and conducting properties of PANI nanofibers, Synth. Met. 162 (2012) 1065–1072, https://doi.org/10.1016/j.synthmet.2012.05.009.

[19] M. Aadil, M. Mahmood, M.F. Warsi, I.A. Alsafari, S. Zulfiqar, M. Shahid, Fabrication of MnO_2 nanowires and their nanohybrid with flat conductive matrix for the treatment of industrial effluents, FlatChem. 30 (2021) 100316, https://doi.org/10.1016/j.flatc.2021.100316.

[20] S. Rahman, M.M. Rahman Khan, B. Deb, S.I. Dana, M.K. Ahmed, Effective and simple fabrication of pyrrole and thiophene-based poly(Py-co-Th)/ZnO composites for high photocatalytic performance, South African, J Chem. Eng. 43 (2023) 303–311, https://doi.org/10.1016/j.sajce.2022.11.010.

[21] M.S.H. Chowdhury, M.M. Rahman Khan, B. Deb, et al., Fabrication of Poly(Ani-co-Py)/NiO composites with superb photocatalytic performance and effective p-nitrophenol sensor, J Inorg. Organomet. Polym. Mater. (2024), https://doi.org/10.1007/s10904-024-03340-9.

[22] A.K. Sibhatu, G.K. Weldegebrieal, S. Sagadevan, N.N. Tran, V. Hessel, Photocatalytic activity of CuO nanoparticles for organic and inorganic pollutants removal in wastewater remediation, Chemosphere. 300 (2022) 134623, https://doi.org/10.1016/j.chemosphere.2022.134623.

[23] M. M. Rahman Khan, S. Cagliero, A. Agostino, M. Beagum, C. Plapcianu, M. Truccato, Control of the oxygen doping in Bi-2212 whiskers by means of their synthesis process, Supercond. Sci. Technol. 22 (2009) 085011. DOI 10.1088/0953-2048/22/8/085011.

[24] R.B. Vasiliev, M.N. Rumyantseva, N.V. Yakovlev, A.M. Gaskov, CuO/SnO_2 thin film heterostructures as chemical sensors to H_2S, Sensors. Actuators B, Chemical. 50 (1998) 186–193, https://doi.org/10.1016/S0925-4005(98)00235-4.

[25] H. Kidowaki, T. Oku, T. Akiyama, Fabrication and characterization of CuO/ZnO solar cell, J Physics: Conference Series. 352 (2012) 012022, https://doi.org/10.1088/1742-6596/352/1/012022.

[26] G.B. Cai, G.X. Zhao, X.K. Wang, S.H. Yu, Direct synthesis of hollow vaterite nanospheres from amorphous calcium carbonate nanoparticles via phase transformation, J. Phys. Chem. C. 114 (2010) 12948–12954, https://doi.org/10.1021/jp801408k.

[27] M. Ikram, A. Khalid, A. Shahzadi, A. Haider, S. Naz, M. Naz, I. Shahzadi, A. Hamid, J. Haider, W. Nabgan, R., Butt Al, enhanced photocatalytic degradation with sustainable CaO nanorods doped with ce and cellulose nanocrystals: in silico molecular docking studies, ACS Omega. 7 (2022) 27503–27515, https://doi.org/10.1021/acsomega.2c02732.

[28] M. Hussain, M. Aadil, E.W. Cochran, S. Zulfiqar, W. Hassan, T. Kousar, H. H. Somaily, F. Mahmood, Facile synthesis of a porous sorbent derived from the rice husk biomass: A new and highly efficient material for water remediation, Inorganic

Chem. Commun. 160 (2024) 112010, https://doi.org/10.1016/j.inoche.2023.112010.
[29] M.M. Baig, M. Hassan, T. Ali, H.M. Asif, A. Asghar, S. Ullah, I.A. Alsafari, S. Zulfiqar, Green 2D simonkolleite/zinc based nanostructures for superior antimicrobial and photocatalytic applications, Mater. Chem. Phys. 287 (2022) 126292, https://doi.org/10.1016/j.matchemphys.2022.126292.
[30] M. Elango, M. Deepa, R. Subramanian, A.M. Musthafa, Synthesis, characterization, and antibacterial activity of polyindole/Ag–CuO nanocomposites by reflux condensation method, Polymer-plastics Technol, Engineer. 57 (2017) 1440–1451, https://doi.org/10.1080/03602559.2017.1410832.
[31] M.M. Rahman Khan, Y.K. Wee, W.A.K. Mahmood, Synthesis of PANI-CaO composite nanofibers with controllable diameter and electrical conductivity, Polym. Compos. 36 (2015) 205–396, https://doi.org/10.1002/pc.22950.
[32] D.M. Fernandes, A.W. Hechenleitner, S.M. Lima, L.H. Andrade, A.R. Caires, Pineda, Preparation, characterization, and photoluminescence study of PVA/ZnO nanocomposite films, Mater. Chem. Phys. 128 (2011) 371–376, https://doi.org/10.1016/j.matchemphys.2011.03.002.
[33] A. Hussain, S. Mehmood, M.N. Rasool, S. Aryal, P. Rulis, W.Y. Ching, Electronic structure, mechanical, and optical properties of $CaO{\cdot}Al_2O_3$ system: a first principles approach, Indian, J Physics. 90 (2016) 917–929, https://doi.org/10.1007/s12648-015-0830-5.
[34] Y. Wang, T. Jiang, D. Meng, J. Yang, Y. Li, Q. Ma, J. Han, Fabrication of nanostructured CuO films by electrodeposition and their photocatalytic properties, Appl. Surf. Sci. 317 (2014) 414–421, https://doi.org/10.1016/j.apsusc.2014.08.144.
[35] L. Xu, G. Zheng, S. Pei, J. Wang, Investigation of optical bandgap variation and photoluminescence behavior in nanocrystalline CuO thin films, Optik. 158 (2018) 382–390, https://doi.org/10.1016/j.ijleo.2017.12.138.
[36] W. Wazir, Z. Ahmad, S. Zulfiqar, E.W. Cochran, S. Mubarik, T. Kousar, H. H. Somaily, J.-J. Shim, H.A. Alsalmah, M. Aadil, Synergistic effects of noble metal doping and nanoengineering on boosting the azo dye mineralization activity of nickel oxide, Ceramics Int. 49 (2023) 38026–38035, https://doi.org/10.1016/j.ceramint.2023.09.133.
[37] A.C. Gandhi, S.Y. Wu, Strong deep-level-emission photoluminescence in NiO nanoparticles, Nanomaterials. 7 (2017) 231, https://doi.org/10.3390/nano7080231.
[38] K.K. Dey, P. Kumar, R.R. Yadav, A. Dhar, A.K. Srivastava, CuO nano ellipsoids for superior physicochemical response of biodegradable PVA, RSC Adv. 4 (2014) 10123–10132, https://doi.org/10.1039/C3RA46898D.
[39] A. Mansur, H. Mansur, J. González, Enzyme-Polymers Conjugated to Quantum-Dots for Sensing Applications, Sensors 11 (2011) 9951–9972, https://doi.org/10.3390/s111009951.
[40] J. Barman, J.P. Borah, K.C. Sarma, Optical properties of chemically prepared CdS quantum dots in polyvinyl alcohol, Int. J. Modern Phys B. 23 (2009) 545–555, https://doi.org/10.1142/S0217979209049917.
[41] I.K. Moon, H. Chun, High transparent thermal curable hybrid polycarbonate films prepared by the sol–gel method, J. Sol-Gel Sci. Technol. 52 (2009) 49–55, https://doi.org/10.1007/s10971- 009-1993-3.
[42] N. Naderi, M.R. Hashim, J. Rouhi, Synthesis and characterization of pt nanowires electrodeposited into the cylindrical pores of polycarbonate membranes, Int. J. Electrochem. Sci. 7 (2012) 8481–8486.
[43] P. Budrugeac, Kinetics of the complex process of thermo-oxidative degradation of poly(vinyl alcohol), J. Therm. Anal. Calorim. 92 (2008) 291–296, https://doi.org/10.1007/s10973-007-8770-8.
[44] M. Aadil, S. Zulfiqar, M.F. Warsi, P.O. Agboola, I. Shakir, Free-standing urchin-like nanoarchitectures of Co_3O_4 for advanced energy storage applications, J. Mater. Res. Technol. 9 (2020) 12697, https://doi.org/10.1016/j.jmrt.2020.08.110.
[45] S. Jabeen, M. Aadil, J. Williams, M.S. Awan, J. Iqbal, S. Zulfiqar, N. Nazar, Synthesis of In_2O_3/GNPs nanocomposites with integrated approaches to tune overall performance of electrochemical devices, Ceramics Int. 47 (2021) 22345–22355, https://doi.org/10.1016/j.ceramint.2021.03.205.
[46] J.W. Gilman, D.L. Van der Hart, T. Kashiwagi, Thermal decomposition chemistry of Poly(vinyl alcohol), ACS Symp. Ser. 599 (1995) 161–185. https://api.semanticscholar.org/CorpusID:19645173.
[47] R. Liu, W. Li, High-thermal-stability and high-thermal-conductivity $Ti_3C_2T_x$MXene/Poly(vinyl alcohol)(PVA) composites, ACS Omega. 3 (2018) 2609–2617, https://doi.org/10.1021/acsomega.7b02001.
[48] A. Leszczynska, J.A.K. Njuguna, K. Pielichowski, J.R. Banerjee, Polymer/montmorillonite nanocomposites with improved thermal properties: Part I. Factors influencing thermal stability and mechanisms of thermal stability improvement, Thermochim. Acta. 453 (2007) 75–96, https://doi.org/10.1016/j.tca.2006.11.003.
[49] R. Singh, S.G. Kulkarni, N.H. Naik, Effect of nano sized transition metal salts and metals on thermal decomposition behavior of polyvinyl alcohol, Adv. Mater. Lett. 4 (2013) 82–88, https://doi.org/10.5185/amlett.2013.icnano.114.
[50] J. Lee, D. Bhattacharyya, A.J. Easteal, J.B. Metson, Properties of nano-ZnO/poly (vinyl alcohol)/poly (ethylene oxide) composite thin films, Curr. Appl. Phys. 8 (2008) 42–47, https://doi.org/10.1016/j.cap.2007.04.010.
[51] Z. Peng, L.X. Kong, S.D. Li, Non-isothermal crystallisation kinetics of self-assembled polyvinylalcohol/silica nano-composite, Polymer. 46 (2005) 1949–1955. https://hdl.handle.net/10536/DRO/DU:30006636.
[52] H.J. Salavagione, G. Martínez, M.A. Gomez, Synthesis of poly(vinyl alcohol)/reduced graphite oxide nanocomposites with improved thermal and electrical properties, J. Mater. Chem. 19 (2009) 5027–5032, https://doi.org/10.1039/B904232F.
[53] A. Zandi, H.A. Ahangar, A. Saffar, Optimization removal of methylene blue from aqueous solution by adsorption on Fe_3O_4@PVA/GT magnetic nanocomposite by Taguchi method, Inorganic Chem. Commun. 158 (2023) 111528, https://doi.org/10.1016/j.inoche.2023.111528.
[54] A. Rahman, S. Zulfiqar, S. Musaddiq, I. Shakir, M.F. Warsi, M. Shahid, Facile synthesis of $Ce_{1-x}Fe_xO_2$/NiO/rGO ternary hybrid heterostructures with enhanced visible light mediated photocatalytic activity for waterborne pollutants, J. Photochem. Photobio A: Chem. 397 (2020) 112583, https://doi.org/10.1016/j.jphotochem.2020.112583.
[55] A. Ihsan, A. Irshad, M.F. Warsi, M.I. Din, S. Zulfiqar, $NiFe_2O_4$/ZnO nanoparticles and its composite with flat 2D rGO sheets for efficient degradation of colored and colorless effluents photocatalytically, Optical Mater. 134 (2022) 113213, https://doi.org/10.1016/j.optmat.2022.113213.
[56] S. Ahmad, M. Aadil, S.R. Ejaz, M.U. Akhtar, H. Noor, S. Haider, I.A. Alsafari, G. Yasmin, Sol-gel synthesis of nanostructured ZnO/$SrZnO_2$ with boosted antibacterial and photocatalytic activity, Ceramics Int. 48 (2022) 2394–2405, https://doi.org/10.1016/j.ceramint.2021.10.020.
[57] A.G. El-Shamy, An efficient removal of methylene blue dye by adsorption onto carbon dot @ zinc peroxide embedded poly vinyl alcohol (PVA/$CZnO_2$) nano-composite: A novel Reusable adsorbent, Polymer. 202 (2020) 122565, https://doi.org/10.1016/j.polymer.2020.122565.
[58] A.M. Omer, W.A. Sadik, A.M. El–Demerdash, et al., Fabrication of semi-interpenetrated PVA/PAMPS hydrogel as a reusable adsorbent for cationic methylene blue dye: isotherms, kinetics and thermodynamics studies, Polym. Bull. 78 (2021) 6649–6673, https://doi.org/10.1007/s00289-020-03456-1.
[59] I. Raheb, M.S. Manlla, Kinetic and thermodynamic studies of the degradation of methylene blue by photo-Fenton reaction, Heliyon 7 (2021) e07427.